

Future ice-sheet surface mass balance and melting in the Amundsen region, West Antarctica.

Marion Donat-Magnin¹, Nicolas C. Jourdain¹, Christoph Kittel², Cécile Agosta³, Charles Amory², Hubert Gallée¹, Gerhard Krinner¹, and Mondher Chekki¹

¹Univ. Grenoble Alpes/CNRS/IRD/G-INP, IGE, Grenoble, France

²F.R.S.-FNRS, Laboratory of Climatology, Department of Geography, University of Liège, B-4000 Liège, Belgium

³Laboratoire des Sciences du Climat et de l'Environnement, IPSL/CEA-CNRS-UVSQ UMR 8212, CEA Saclay, F-91190, Gif-sur-Yvette, France

Correspondence: Nicolas C. Jourdain (nicolas.jourdain@univ-grenoble-alpes.fr)

Abstract. We present projections of West-Antarctic surface mass balance (SMB) and surface melting in 2080-2100, under the rcp8.5 scenario and based on a 10-km regional model. Our projections are built by adding a CMIP5 (5th Coupled Model Intercomparison Project) multi-model-mean seasonal climate-change anomaly to the present-day model boundary conditions. Using an anomaly has the advantage to reduce CMIP5 model biases, and a perfect-model test reveals that our approach captures 5 most characteristics of future changes, despite a 16-17% underestimation of projected SMB and melt rates.

SMB over the grounded ice sheet in the sector between Getz and Abbot increases from 336 Gt.yr⁻¹ in 1989-2009 to 455 Gt.yr⁻¹ in 2080-2100, which would reduce the global sea level changing rate by 0.33 mm.yr⁻¹. Snowfall indeed increases by 8.5 to 10.5% per °C of near-surface warming, due to increasing air water-holding capacity in warmer conditions, reduced sea-ice concentrations, and more marine air intrusion.

10 Ice-shelf surface melt rates increase by an order of magnitude along the 21st century, due to increased humidity and subsequent downward longwave radiation, and to reduced albedo in the presence of melting. Eastern ice shelves (Abbot, Cosgrove and Pine Island) experience significant runoff in the future, while western ice shelves (Thwaites, Crosson, Dotson and Getz) remain without runoff. This is explained by the evolution of the melt-to-snowfall ratio: below a threshold of 0.60 to 0.85, snowfall brings too much porosity to be filled by melt water, while firn air depletion and runoff occur for higher ratios. This suggests 15 that western ice shelves might remain unaffected by hydrofracturing for more than a century under rcp8.5, while eastern ice shelves may experience hydrofracturing before the end of this century.

Copyright statement. TO BE COMPLETED

1 Introduction

In a perfectly stable climate, the Antarctic ice sheet would have a constant mass, and the Surface Mass Balance (SMB, the sum 20 of rainfall and snowfall minus sublimation, runoff and eroded snow) over the grounded ice sheet, i.e. 1800 to 1900 Gt.yr⁻¹

under the present climate (van Wessem et al., 2018; Agosta et al., 2019), would be exactly compensated by the ice flow across the grounding line, i.e., into the ocean. In contrast to this hypothetically stable climate, the Antarctic ice sheet has lost 2720 ± 1390 Gt of grounded ice from 1992 to 2017, which corresponds to 7.6 ± 3.9 mm of sea level rise (Shepherd et al., 2018). The main origin of the current mass loss is the acceleration of major ice streams (Bamber et al., 2018; Shepherd et al., 2018; 5 Rignot et al., 2019), mostly driven by increased oceanic melt (e.g. Turner et al., 2017; Jenkins et al., 2018). In a warmer climate, SMB may significantly increase and partly compensate the loss due to accelerated ice flows (e.g. Favier et al., 2017).

Current SMB trends (1979–2000) are slightly negative, with SMB decreasing at a rate of -2.7 ± 3.8 Gt.yr $^{-2}$ for the entire ice sheet, and large differences between West Antarctica (-0.1 ± 1.4 Gt.yr $^{-2}$) and East Antarctica (-4.5 ± 3.5 Gt.yr $^{-2}$) (Medley and Thomas, 2019). These trends only represent a small fraction of the current ice-sheet imbalance (-110 Gt.yr $^{-1}$ over 1992–10 2017), but climate models predict a significant increase in Antarctic precipitation over the 21st century (Kriinner et al., 2007; Genton et al., 2009; Nowicki et al., 2020). Under the A1B or RCP8.5 scenarios to 2100, simulated SMB are increased by 13 to 25% depending on the climate model (Agosta et al., 2013; Ligtenberg et al., 2013; Lenaerts et al., 2016; Palerme et al., 2017). These changes are strongly related to temperatures (Frieler et al., 2015), with a SMB sensitivity of 5–7% per degree 15 of near-surface warming (Kriinner et al., 2008; Ligtenberg et al., 2013; Agosta et al., 2013; Palerme et al., 2017). In a warmer climate, the water-holding capacity of the troposphere indeed increases (Clapeyron, 1834; Clausius, 1850), and more humidity can be transported and made available for Antarctic precipitation.

Runoff is a negative contribution to SMB, and it can possibly trigger ice-shelf collapse through hydrofracturing or ice-shelf bending (e.g. Bell et al., 2018). It is produced if surface melt or rain rates are high enough to percolate and fill the pore space in the snow and firn layers, which is sometimes referred to as firn air depletion (Pfeffer et al., 1991; Kuipers Munneke et al., 20 2014). Currently, runoff is two orders of magnitude smaller than precipitation for the entire Antarctic ice sheet (van Wessem et al., 2018; Agosta et al., 2019). Surface melting only occurs to a significant extent over the Peninsula (Scambos et al., 2009; Trusel et al., 2013), and sporadically in other regions like the Amundsen Sea (Nicolas et al., 2017; Donat-Magnin et al., 25 2020) and Ross Sea (Bell et al., 2017) sectors. Over most ice shelves in Antarctica, current melt rates are too low compared to snowfall (bringing porosity), and there is no significant firn air depletion and subsequent runoff (Kuipers Munneke et al., 2014). An exception is the Western side of the Antarctic Peninsula that experienced melt water ponds and the resulting collapse 20 of Larsen B ice shelf (van den Broeke, 2005; Scambos et al., 2009; Vaughan et al., 2003), and where simulations suggest nearly depleted firn air (Kuipers Munneke et al., 2014).

In a warmer climate, surface melting is expected to increase, potentially leading to higher mass loss through runoff and to the occurrence of melt water ponds, hydrofracturing and subsequent ice-shelf collapse. Surface melt rates increase exponentially 30 with surface air temperature, which is explained by increased duration of the melt season, positive melt-albedo feedback, and increased downward longwave radiations and turbulent heat fluxes (Kuipers Munneke et al., 2014; Trusel et al., 2015). As near-surface air temperatures are projected to increase in Antarctica (e.g. Bracegirdle et al., 2008), melting is expected to become more common in response to increased anthropogenic emissions. Based on a firn model forced by regional atmospheric 35 simulations constrained by global projections, Kuipers Munneke et al. (2014) estimated that a few more ice shelves could experience near-complete firn air depletion by 2100, and many more ice shelves by 2200 in East and West Antarctica under

the strongest emission scenario. Using regional atmospheric simulations and global projections with bias corrections, Trusel et al. (2015) reported that large fractions of East and West Antarctic ice shelves could experience melt rates greater than the pre-collapse value of Larsen B by the end of the 21st century under the warmest scenario.

Computing projections of future SMB and surface melt rates remains challenging, because of the strong natural variability at 5 regional scales (Lenaerts et al., 2016; Donat-Magnin et al., 2020), biases in global climate models (GCMs) (Bracegirdle et al., 2013; Swart and Fyfe, 2012) and GCM resolutions that are too coarse to resolve the orographic processes in the relatively steep coastal area (Krinner et al., 2008; Lenaerts et al., 2012). Most models that participated in the 5th Climate Model Intercomparison Project (CMIP5 Taylor et al., 2012) overestimated the present-day Antarctic SMB, by more than 100% in some cases (Palerme et al., 2017). These models also had a generally poor representation of the snow-pack energy balance, which is why future melt 10 rate estimates have often been derived from simulated air temperatures rather than directly provided by the models (Davies et al., 2014; Trusel et al., 2015). These limitations remain in most CMIP6 models (REF SnowMIP?). Recent versions of regional climate models (RCMs) with a comprehensive representation of polar processes are now able to simulate melt rates in reasonable agreement with observational estimates (Lenaerts et al., 2018; Datta et al., 2019; Donat-Magnin et al., 2020). Using this kind of RCMs to downscale projections from GCMs can significantly reduce surface biases (Lang et al., 2015). 15 However, this approach is not sufficient to remove the large-scale biases inherited from GCMs, and bias corrections may be needed (Trusel et al., 2015; Beaumet et al., 2019a). In this paper, we build SMB and surface melting projections at the end of the 21st century by forcing an RCM with the 3-dimensional climate-change anomalies from a CMIP5 rcp8.5 multi-model mean with the aim of removing a part of the CMIP model biases (see section 2).

We focus on the Amundsen Sea sector, where potential future melt-induced hydrofracturing and associated loss of ice- 20 shelf buttressing could have large effects on the stability of the West Antarctic ice sheet, with strong impact on sea level rise. Currently the Amundsen sector accounts for 60% of the total Antarctic mass loss (Rignot et al., 2019). While oceanic melt is currently the dominant process that causes mass loss (Thoma et al., 2008; Turner et al., 2017; Jenkins, 2016; Jenkins et al., 2018), surface air temperature is expected to increase (Bracegirdle et al., 2008), and whether the ice shelves of the 25 Amundsen sectors will respond with the same hydrofracturing mechanism as in the Antarctic Peninsula remains an open question as contrasting behaviours were projected for individual ice shelves in previous studies at relatively coarse resolution (Kuipers Munneke et al., 2014; Trusel et al., 2015). In the following, we describe our general methodology (section 2), then we assess our projection method through a perfect-model approach (section 3), and we describe future projections with a particular focus on surface mass balance over the grounded ice sheet and melting over the ice shelves (section 4). We also discuss the impact of model biases, and propose an extrapolation of our results to other scenarios or time horizons (section 5).

30 2 Method

2.1 Regional atmosphere and firn model

Our projections of the West Antarctic surface climate for the end of the 21st century are based on version 3.9.3 of the MAR regional atmospheric model (Gallée and Schayes, 1994; Agosta et al., 2019). Our regional configuration is centered on the

Amundsen Sea sector, covers 2800×2400 km, and was developed by Donat-Magnin et al. (2020). The horizontal resolution is 10 km and we use 24 vertical sigma levels located from approximately 1 m to 15500 m above the ground. The snow pack is represented by 30 layers of snow/firn covering the first 20 m with refined resolution at the surface (1 mm). The topography is derived from BEDMAP2 (Fretwell et al., 2013) and the drainage basins used for averages were defined by Mouginot et al. 5 (2017).

The radiative scheme and cloud properties are the same as in Datta et al. (2019) and the surface scheme, including snow density and roughness, are the same as in Agosta et al. (2019). The atmosphere is coupled to the SISVAT surface scheme (Soil Ice Snow Vegetation Atmosphere Transfer De Ridder and Gallée, 1998), which is a multi-layer model that includes prognostic equations for temperature, mass, water content and snow properties (i.e. dendricity, sphericity and grain size). SISVAT and the 10 atmosphere are coupled through exchanges of radiative and turbulent heat fluxes.

Surface albedo depends on the evolving snow properties and on the solar zenithal angle. As in Agosta et al. (2019), the density of fresh snow increases with wind speed ($+6.84 \text{ kg.m}^{-3}.(\text{m.s}^{-1})^{-1}$) and temperature ($+0.48 \text{ kg.m}^{-3}.^{\circ}\text{C}^{-1}$). In case of surface melting or rainfall, liquid water percolates downward into the next snow/firn layers, with a water retention of 10% of the porosity in each successive layer. Layers reaching a close-off density of 830 kg.m^{-3} become non-permeable (CHECK 15 IN CODE: DOES IT ACTUALLY PREVENT THE WATER FROM GOING FURTHER DOWN??). If the liquid water is not able to percolate further down, then it fills the entire porosity of the surface layers, and the excess is counted as runoff. As in Agosta et al. (2019), our set-up does not include blowing snow, which is not considered as a strong limitation for this sector of Antarctica (Lenaerts et al., 2012), although this remains a poorly quantified process.

2.2 Present-day and future forcing

20 The simulation representative of the present climate is the same as in Donat-Magnin et al. (2020). It is forced laterally (pressure, wind, temperature, specific humidity), at the top (i.e. above 200 hPa) of the troposphere (temperature, wind), and at the surface (sea ice concentration, sea surface temperature) by 6-hourly outputs of the ERA-interim reanalysis (Dee et al., 2011), which has a good representation of the Antarctic climate (Bromwich et al., 2011; Huai et al., 2019). A thorough evaluation of the present-day simulation with respect to in-situ and satellite observational products is provided in Donat-Magnin et al. (2020).
25 In this paper, we do not describe or discuss features located eastward of $\sim 75^{\circ}\text{W}$ (e.g. Georges VI ice shelf) and southward of 78°S (e.g. Ross and Ronne ice shelves) as this is considered too close to the sponge zone where lateral boundary conditions are prescribed and where model solutions are known to be dubious.

For the future, we calculate the 3-dimensional climate-change absolute anomaly from a CMIP5 multi-model mean (MMM), and we add it to the 6-hourly ERA-interim variables used to force MAR, i.e. sea surface temperature (SST), sea ice cover 30 (SIC), wind velocity, air temperature and humidity. The MMM anomaly is defined as the mean difference between 1989-2009 and 2080-2100 (under the rcp8.5 emission scenario), for an ensemble of 33 CMIP5 models: ACCESS1-0, ACCESS1-3, BNU-ESM, CCSM4, CESM1-BGC, CESM1-CAM5, CESM1-WACCM, CMCC-CESM, CMCC-CMS, CMCC-CM, CNRM-CM5, CSIRO-Mk3-6-0, CanESM2, FGOALS-g2, FIO-ESM, GFDL-CM3, GFDL-ESM2G, GFDL-ESM2M, HadGEM2-CC, HadGEM2-ES, IPSL-CM5A-LR, IPSL-CM5A-MR, IPSL-CM5B-LR, MIROC-ESM-CHEM, MIROC-ESM, MIROC5, MPI-

ESM-LR, MPI-ESM-MR, MRI-CGCM3, NorESM1-ME, NorESM1-M, bcc-csm1-1, inmcm4, taking the first available ensemble member for each model (i.e. “r1i1p1” or “r2i1p1” if not available). The anomaly is calculated separately for each calendar month, meaning that we apply an anomaly that includes a seasonal cycle. Monthly anomalies are linearly interpolated between two given dates to avoid discontinuity. In the future simulation, we do not increase greenhouse gases concentrations
5 in our regional domain, which is expected to have a minor effect because the dominant effect of global increase in greenhouse gases concentrations on our simulations comes from changes in sea surface and sea ice forcing as well as through increased temperature and humidity at the lateral boundaries (Bull et al., 2020).

Adding an anomaly is relatively simple, but requires a specific calculation for two variables. First, specific humidity is set to zero in the rare cases where applying the CMIP5 anomaly would produce unphysical negative values. Second, sea-ice
10 concentration (SIC) anomalies are applied through an iterative process, which is needed because some locations have non-zero SIC on some days, and zero SIC on other days. As negative SIC values are unphysical, applying a negative climatological SIC anomaly to all days (but keeping days with zero SIC unchanged) does not conserve the applied CMIP5 anomaly. To circumvent this issue, we apply the anomaly through 20 iterations: we start applying the CMIP5-MMM anomaly to the days and locations
15 with SIC greater than zero (for negative anomaly) and smaller than 100% (for positive anomaly), and after each iteration, we calculate the residual SIC that would be needed to reach the original CMIP5-MMM SIC anomaly, and we add it to the applied climatological anomaly. The effect of this sea-ice anomaly correction is briefly described in section 3. Alternative sea-ice correction methods were evaluated by Beaumet et al. (2019b), but here we prefer to stay as close as possible to the simple anomaly method used for the other variables.

As discussed by Knutti et al. (2010), the MMM is often considered as the “best” estimate for future climate because individual model biases are partly canceled in the MMM, although an equal weight for all the models does not account for the fact that models are not independent from each other because of the same operating centers, common history, shared physical parameterizations and numerical methods (Knutti et al., 2017; Herger et al., 2018). Given that the CMIP model biases are largely stationary even under strong climate changes (Krinner and Flanner, 2018), our method is also expected to remove a part of the biases in individual models. This method has previously been used in other regions (e.g. Knutson et al., 2008; Walsh,
25 2015; Dutheil et al., 2019) but, to our knowledge, never in Antarctica. A similar method was used by Krinner et al. (2008) in global simulations with a stretched grid over Antarctica, which only involved anomalies in the sea surface conditions.

All the simulation years are run in parallel with a 12-year spin up for each simulated year, which is sufficient to obtain a steady runoff in the future simulation over all ice shelves except Abbot (see Discussion). When not stated otherwise, the present-day period represents 1988-2017. The future anomaly corresponds to the 1988-2017 period to which has been added
30 the CMIP5-MMM anomaly (2080-2100 minus 1989-2009) and therefore represents something like 2079-2108 (with the inter-annual variability of 1988-2017). While our CMIP5-MMM anomaly is only based on 21 years, we decided to run our regional simulations over 30 years, which provides more statistical significance given that surface melt rates and SMB exhibit high interannual variability in this region (Scott et al., 2019; Donat-Magnin et al., 2020).

We now briefly describe the CMIP5-MMM anomalies applied to ERAinterim. The troposphere is warmed relatively uniformly from the surface to \sim 300 hPa (Fig. 1a). There is a clear seasonal cycle in the low-troposphere anomalies, with stronger
35

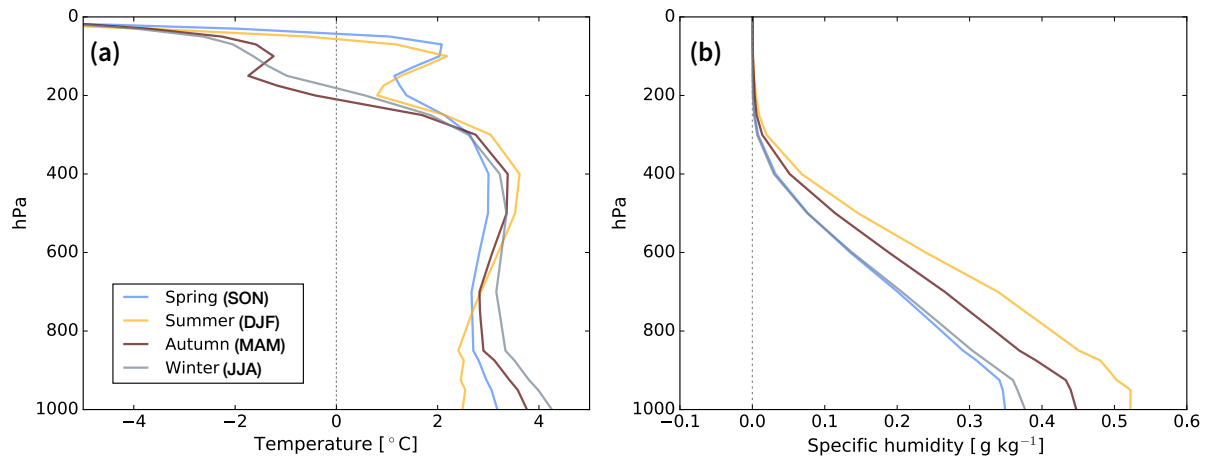


Figure 1. (a) temperature and (b) specific humidity vertical profiles of the CMIP5-MMM anomaly (2080-2100 minus 1989-2009) that is added to ERA-interim, here spatially-averaged over West Antarctica (60-85°S , 170-40°W).

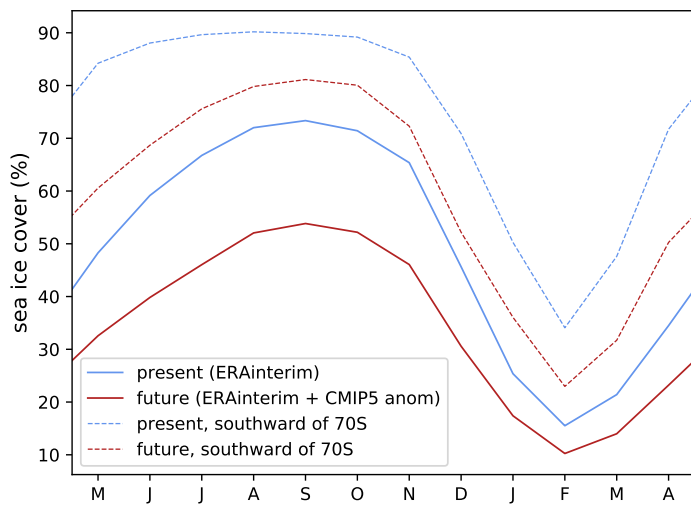


Figure 2. Mean seasonal cycle of sea-ice concentration over the oceanic part of the MAR domain (solid) and southward of 70°S (dashed), for the present-day (blue) and future (dark-orange) simulations.

warming in winter than in summer. This is related to stronger changes in winter sea-ice concentration compared to summer (solid lines in Fig. 2), because present-day summers are already relatively sea-ice free and, as such, cannot decrease much further. As expected from the radiative effects of greenhouse gases, the stratosphere tends to cool in response to increased anthropogenic emissions of greenhouse gases (e.g. Seidel et al., 2011). There is also a clear seasonal cycle in the lower stratosphere (~ 100 hPa), with future warming in spring and summer and cooling in the other seasons, which may be related to seasonal effects of ozone recovery (Perlitz et al., 2008). Specific humidity increases as the troposphere warms (Fig. 1b), as expected from the Clausius-Clapeyron relation.

3 Assessment of the projection method

In this section, we assess the ability of our projection method to capture the future climatology. To do so, we now consider a single model, namely ACCESS-1.3 (Bi et al., 2013; Lewis and Karoly, 2014), which reproduces remarkably well the present-day climate over Antarctica (Agosta et al., 2015; Naughten et al., 2018; Barthel et al., 2020). We first run MAR forced by ACCESS-1.3 over 1989-2009 and 2080-2100 under the rcp8.5 scenario, and we consider 2080-2100 as the true future. Then, we calculate the seasonal climatological anomaly and add it to the present-day interannual forcing, i.e. following the methodology described in the previous section but using present-day ACCESS-1.3 and its future anomalies instead of ERAinterim and the CMIP5 MMM anomaly. The future based on the absolute anomaly method is referred to as *projected future* in this section, and it is compared to the *true future* (i.e. from the direct downscaling of ACCESS-1.3) to evaluate our projection method.

The fidelity of our projection method is assessed by comparing the difference between the *projected future* and the *true future* (referred to as projection bias) to the true climate change signal (*true future* minus present). We can see that our iterative sea-ice correction (see section 2) is effective, reducing the SIC projection bias from 14% to 0.3% of the climate-change anomaly in SON, and from 40% to 20% of the climate-change anomaly in DJF (Fig. 3a).

Over the ice-sheet, the projection biases are 0.6°C in JJA and 0.2°C in DJF, which is relatively small compared to a warming signal of 3.5°C and 3.0°C for these two seasons respectively (Fig. 3b). Looking at the peak melt rate in January (Fig. 3c), we find that the projection bias represents 17% of the climate-change signal, vs 34% if no iterative method is used for sea ice (Fig. 3d).

In terms of spatial pattern, the SMB projection bias is relatively noisy, possibly reflecting different synoptic variability between the *true future* and the *projected future* (Fig. 4a,b). The climate change signal nonetheless remains significantly larger than the projection bias at most locations. The melt projection bias is positive at most melting locations, with a bias consistently smaller than the climate change signal (Fig. 4c,d).

To summarize, our projection method has the advantage to start from a present-day state that is not affected by present-day biases in CMIP5 models and to be applicable to a multi-model-mean projection, which is expected to remove a part of the CMIP5 model biases. The counterpart of these advantages are biases in the projection itself. These biases are estimated to reach 17% based on our perfect-model approach. A part of these biases may be related to the imperfect method used to apply

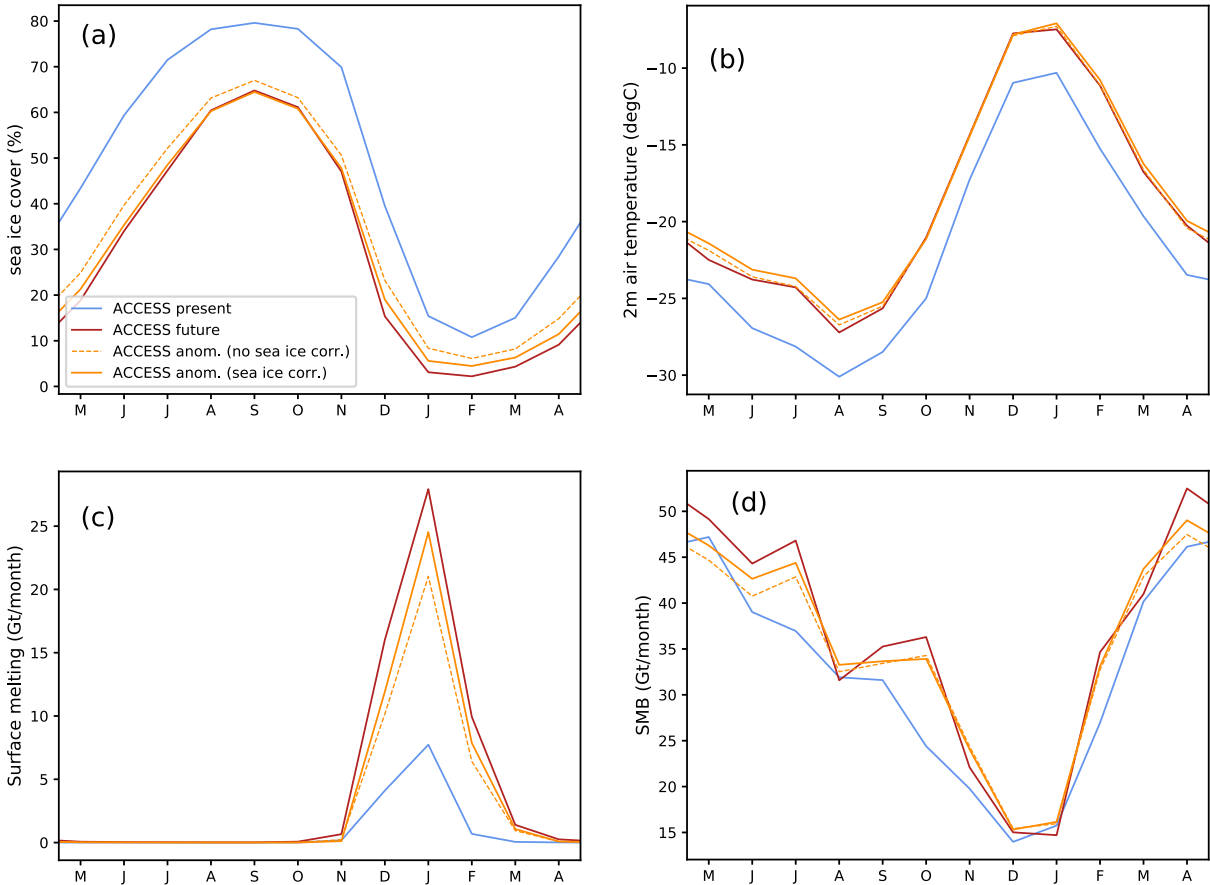


Figure 3. Mean 21-year seasonal cycle of: (a) domain-averaged sea-ice concentration, (b) 2 m air temperature, (c) surface melting and (d) SMB, with (b-d) integrated over the seven glacial drainage basins from Getz to Abbot (both ice shelf and grounded ice). The blue and dark-red lines correspond to the present and *true future* based on ACCESS-1.3, respectively. The orange lines represent the results of the *projected future*, applied with (solid) and without (dashed) sea-ice iterative correction (see section 2).

the sea-ice anomaly. Using iterative absolute anomalies typically removes half of the projection biases compared to a simple absolute anomaly, but the bias is not completely removed in summer, and more iterations may be needed in our approach. Alternative approaches to build future sea-ice concentrations were proposed by Beaumet et al. (2019b), and some of them may be more effective at removing projection biases, although their approaches produced biases of similar magnitude as our 5 iterative absolute anomaly method (their Fig. 5). Another possible cause for our projection biases is the fact that we assume unchanged interannual variability with respect to the mean in the *projected future*, while the *true future* experiences a different variability. Changes in interannual variability may indeed affect non-linear processes (e.g., melt rates vary exponentially with temperatures) even if the mean is the same in the true future and the future from the anomaly method.

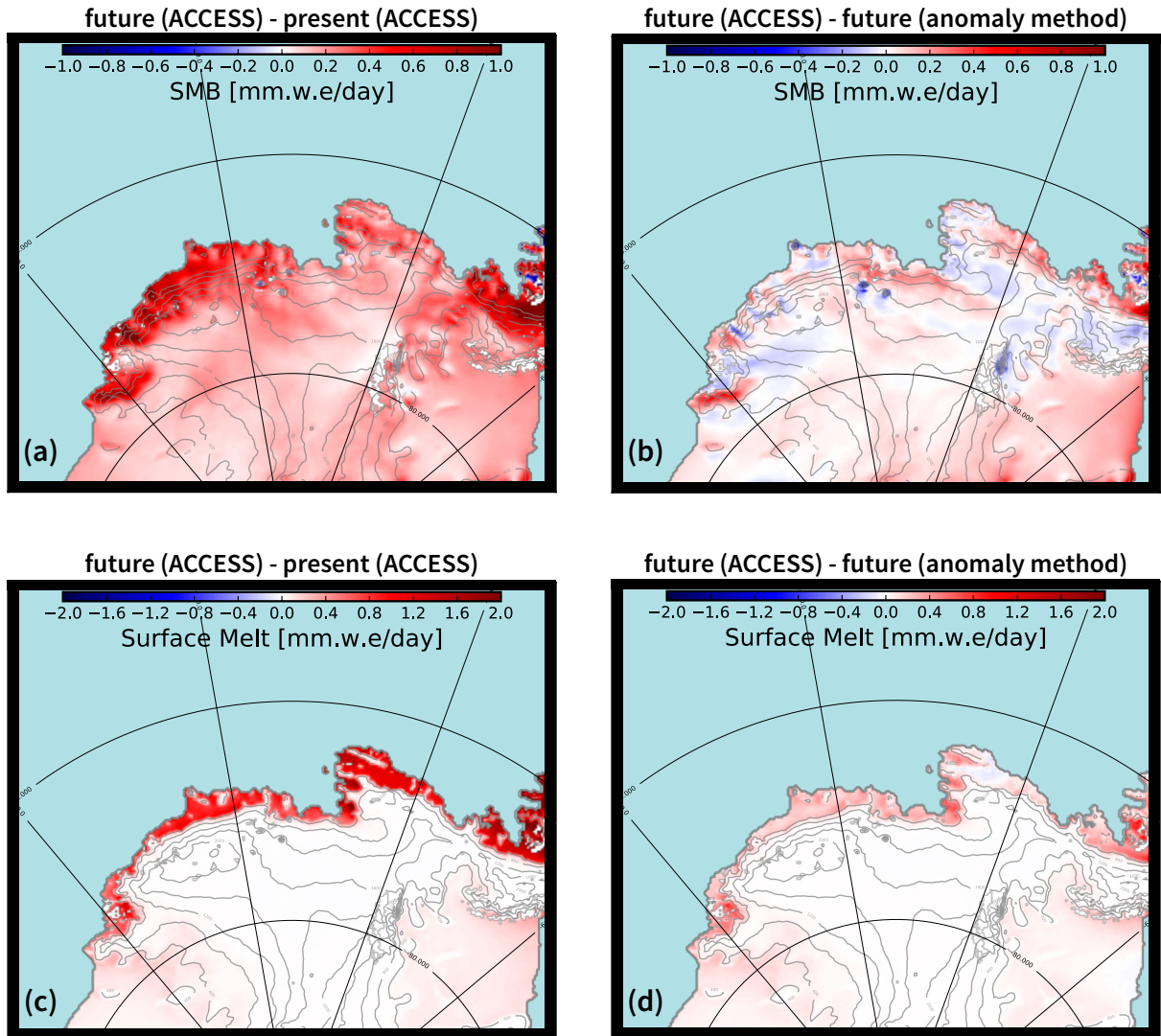


Figure 4. (a) SMB anomaly (2080-2100 minus 1989-2009) in ACCESS-1.3 directly downscaled by MAR (i.e. *true* changes). (b) Same as (a) but with a future simulation derived from the anomaly method applied to ACCESS-1.3 (i.e. *projected* changes). (c-d) Same as (a-b) but for melt rates instead of SMB. The ocean is in light blue, and the ice-sheet topography is shown in gray (contours every 400 m).

Table 1. SMB and its components over the grounded part of individual glacial drainage basins (Gt.yr^{-1}), for present day (regular) and future (bold). SMB is the sum of snowfall and rainfall minus sublimation and runoff.

| SMB component | Abbot | Cosgrove | Pine Island | Thwaites | Crosson | Dotson | Getz |
|---------------|-------------|-------------|--------------|--------------|-------------|-------------|--------------|
| SMB | 36.3 | 7.1 | 80.1 | 95.9 | 20.6 | 16.9 | 79.3 |
| | 50.8 | 10.0 | 110.2 | 129.1 | 28.4 | 22.9 | 103.5 |
| Snowfall | 37.0 | 7.3 | 82.0 | 95.6 | 21.0 | 17.3 | 81.0 |
| | 50.5 | 10.0 | 111.3 | 127.7 | 28.6 | 23.2 | 104.5 |
| Rainfall | 0.1 | 0.0 | 0.1 | 0.0 | 0.1 | 0.0 | 0.0 |
| | 0.7 | 0.1 | 0.3 | 0.1 | 0.2 | 0.1 | 0.2 |
| Sublimation | 0.7 | 0.2 | 2.0 | -0.2 | 0.5 | 0.4 | 1.7 |
| | 0.4 | 0.1 | 1.1 | -1.3 | 0.4 | 0.3 | 1.2 |
| Runoff | 0.0 | 0.0 | 0.0 | 0.0 | 0.0 | 0.0 | 0.0 |
| | 0.1 | 0.0 | 0.3 | 0.0 | 0.0 | 0.0 | 0.0 |

Notwithstanding these limitations, we consider that our methodology has some advantages and should be used for projections together with other existing methods. We therefore apply it to ERAinterim and CMIP5 MMM in the following section.

4 Projections

In this section, we present SMB and surface melting projections derived from ERAinterim and the CMIP5-MMM-rcp8.5 anomaly. We simply refer to the corresponding simulations as “present” and “future” in the following. We also investigate the causes for these changes and we discuss possible consequences for hydrofracturing and sea level rise.

4.1 Grounded ice-sheet SMB

The future SMB is increased by 30 to 40%, keeping a very similar pattern to present day (Fig. 5a,b), i.e. mostly controlled by the steep slopes and local topographic features near the ice-sheet margin. Considering the grounded part (which matters for sea level rise) of all the drainage basins from Getz to Abbot (boundaries indicated in Fig. 5a), SMB increases from 336 Gt.yr^{-1} presently to 455 Gt.yr^{-1} at the end of the 21st century (Tab. 1). As previously reported by Ligtenberg et al. (2013), increasing snowfall explains most of the SMB changes. Projected sublimation slightly decreases in all basins, while rainfall slightly increases, but both components remain two orders of magnitude smaller than snowfall. Runoff is projected to remain near zero over the grounded ice sheet in this sector.

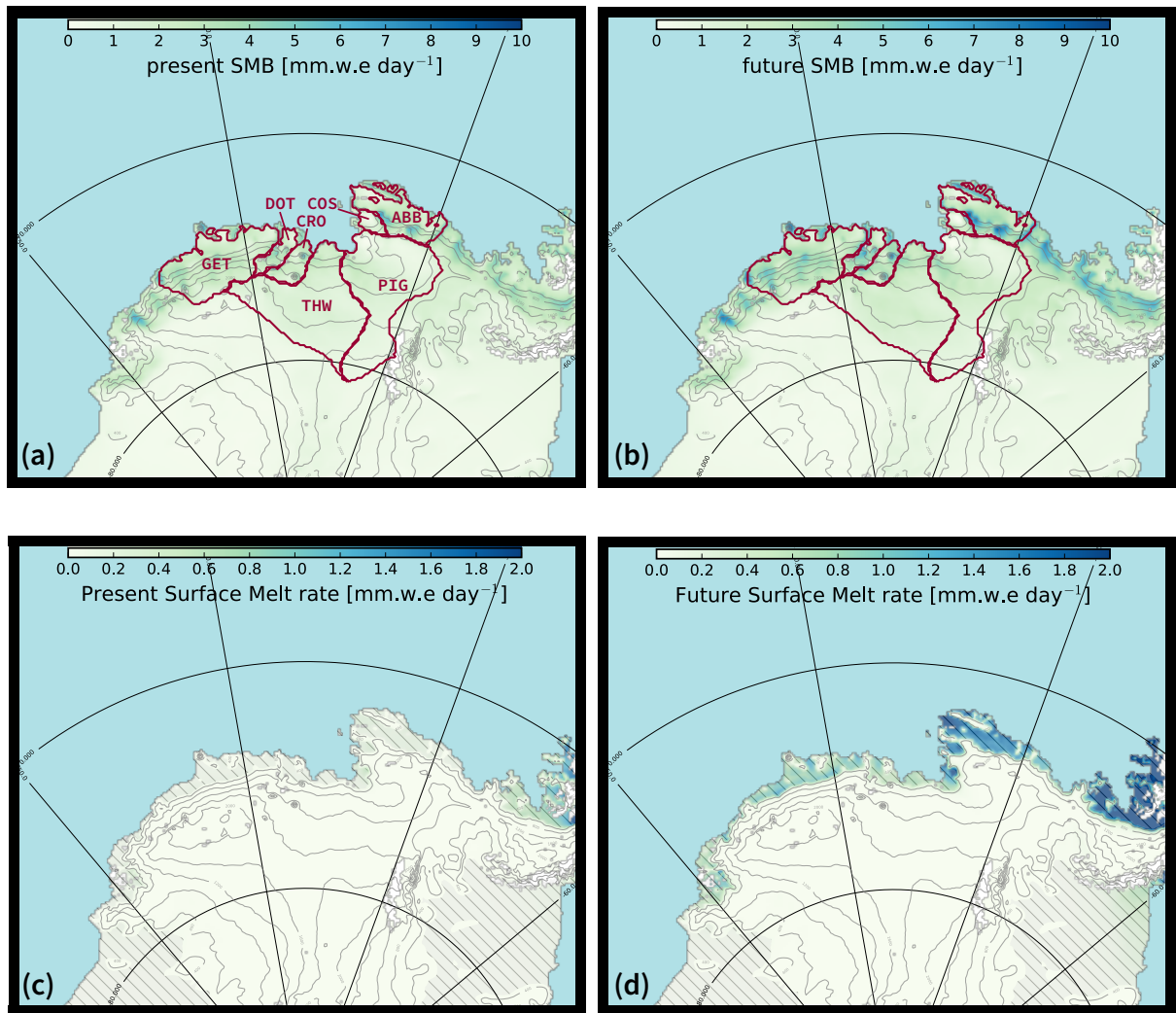


Figure 5. (a) Present-day and (b) future annual mean SMB. (c) Present-day and (d) future annual mean melt rates. The red contours in the upper panel indicate individual glacial drainage basins. Hatching in the lower panels indicate ice shelves. The ocean is in light blue, and the ice-sheet topography is shown in gray (contours every 400 m).

We now briefly analyze possible causes for increased SMB in a warmer climate. The water-holding capacity increases with air temperature, at a rate of $\sim 7.5\% \cdot ^\circ\text{C}^{-1}$ at temperatures typical of coastal Antarctica (Clausius-Clapeyron relation). In our simulations, near surface warming reaches 3.4 to 3.7°C for the various basins, which is very close to the rcp8.5 MMM global warming value (Collins et al., 2013). The corresponding increase in snowfall over the grounded ice sheet represents +8.5 to 5 + $10.5\% \cdot ^\circ\text{C}^{-1}$, which is higher than the theoretical Clausius-Clapeyron rate, and higher than previous estimates by Ligtenberg et al. (2013) and Palmer et al. (2017) for the entire Antarctic ice sheet. This indicates that other factors may contribute to increasing SMB in the Amundsen sector.

To further understand the mechanism for increased snowfall, we now consider projections for the four seasons separately (Fig. 6). The strongest increase in SMB occurs in MAM (followed by JJA), which corresponds to the season with largest 10 changes in sea-ice concentrations in the vicinity of the ice-sheet margin (see dashed lines in Fig. 2). While Clausius-Clapeyron refers to the maximum water-holding capacity, we suggest that decreasing coastal sea-ice cover makes surface air masses closer to their saturation level. Another possible contributor to increased snowfall is the changing low-troposphere circulation, which shows a cyclonic anomaly in MAM, favoring southward humidity transport (Fig. 7).

4.2 Ice-shelf surface melting and runoff

15 We have shown that runoff plays no significant role in the grounded-ice-sheet SMB and therefore on sea level projections. However, surface melting and subsequent runoff may lead to melt water ponding over ice shelves and trigger hydrofracturing. In this section, we therefore focus on surface melting and runoff projections over the seven major ice shelves from Getz to Abbot.

On average over the seven major ice shelves from Getz to Abbot, surface melt rates are projected to increase from several 20 tens to several hundreds of mm.w.eq.yr^{-1} , and melt occurrence is projected to increase from typically a week per year to 1-2 months per year (Tab. 2). As previously noticed by Kuipers Munneke et al. (2014) and Trusel et al. (2015), we find an exponential dependency of melt rates to 2 m air temperatures (not shown), which explains relatively strong increases in melt rates compared to SMB. In terms of seasonality, future melt rates are strongly increased in summer (DJF) over all the ice shelves, while Abbot, Cosgrove and Pine Island also experience significantly more melting in fall and spring (Fig. 8).

25 Rainfall is also projected to increase (Tab. 2), but represents a relatively small fraction of surface melting (less than 15% for all the ice shelves). Interestingly, future surface melting and rainfall entirely refreeze in the firn for all the ice shelves from Getz to Thwaites, which leads to no runoff in the future. In contrast, Abbot, Cosgrove and Pine Island produce some runoff, although most surface melting and rainfall also refreeze in the firn.

To explain this contrast between western (Getz to Thwaites) and eastern (Pine Island to Abbot) ice shelves, we show how 30 runoff evolves with the melt-to-snowfall ratio (Fig. 9). Considering a very simple snow/firn model, Pfeffer et al. (1991) suggested that surface melting would lead to firn-air depletion for melt-to-snowfall ratios greater than approximately 0.7 (for fresh-snow and close-off densities of 300 and 830 kg.m^{-3} respectively). For smaller ratios, the porosity brought by snowfall exceeds the porosity filled by snow melting. Here we notice some variability due to the more complex firn model in MAR, with episodic runoff for annual melt-to-snowfall ratios as low as 0.25, and a very high probability of runoff for annual melt-

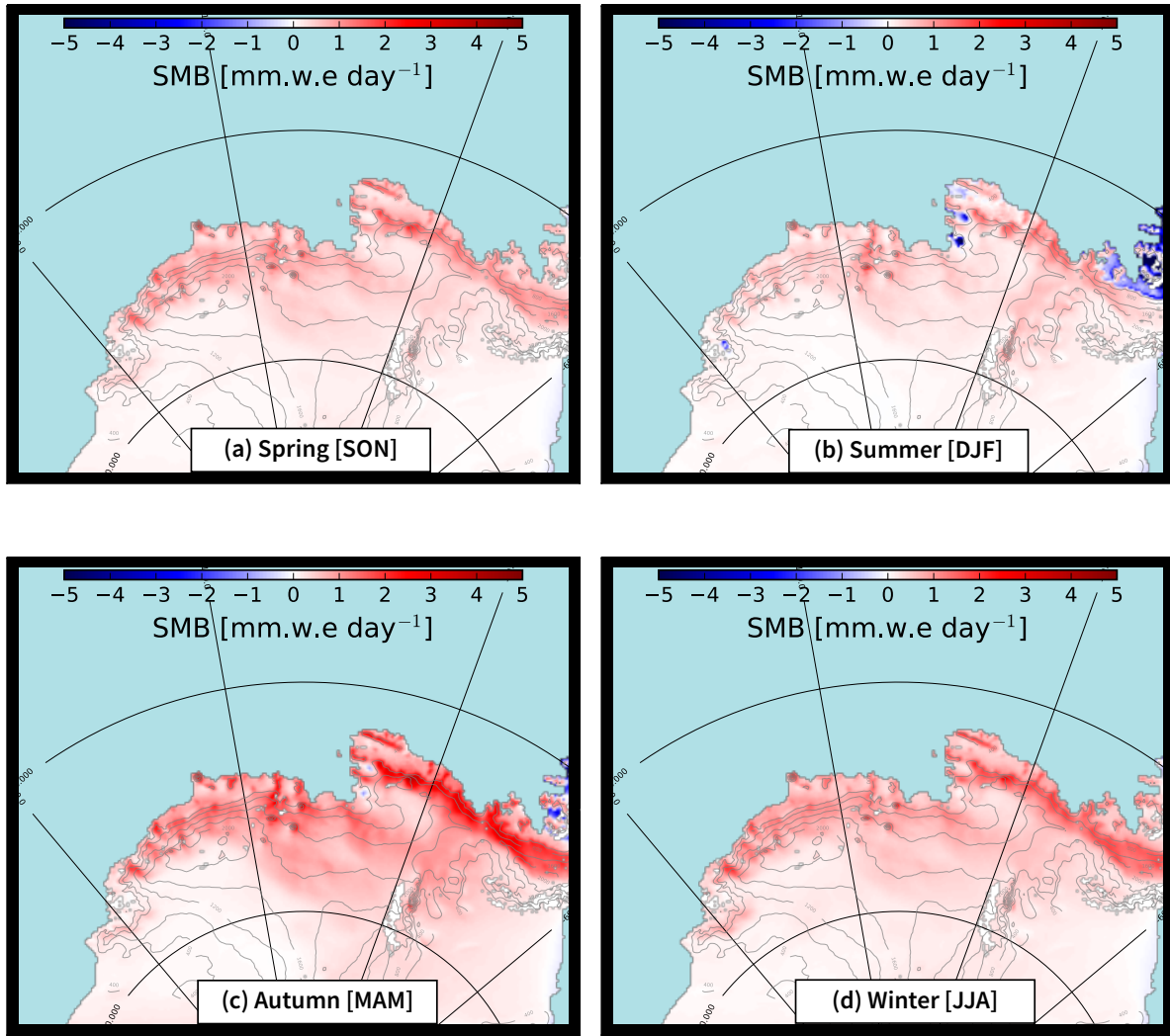


Figure 6. Changes in mean seasonal SMB (future minus present). The ocean is in light blue, and the ice-sheet topography is shown in gray (contours every 400 m).

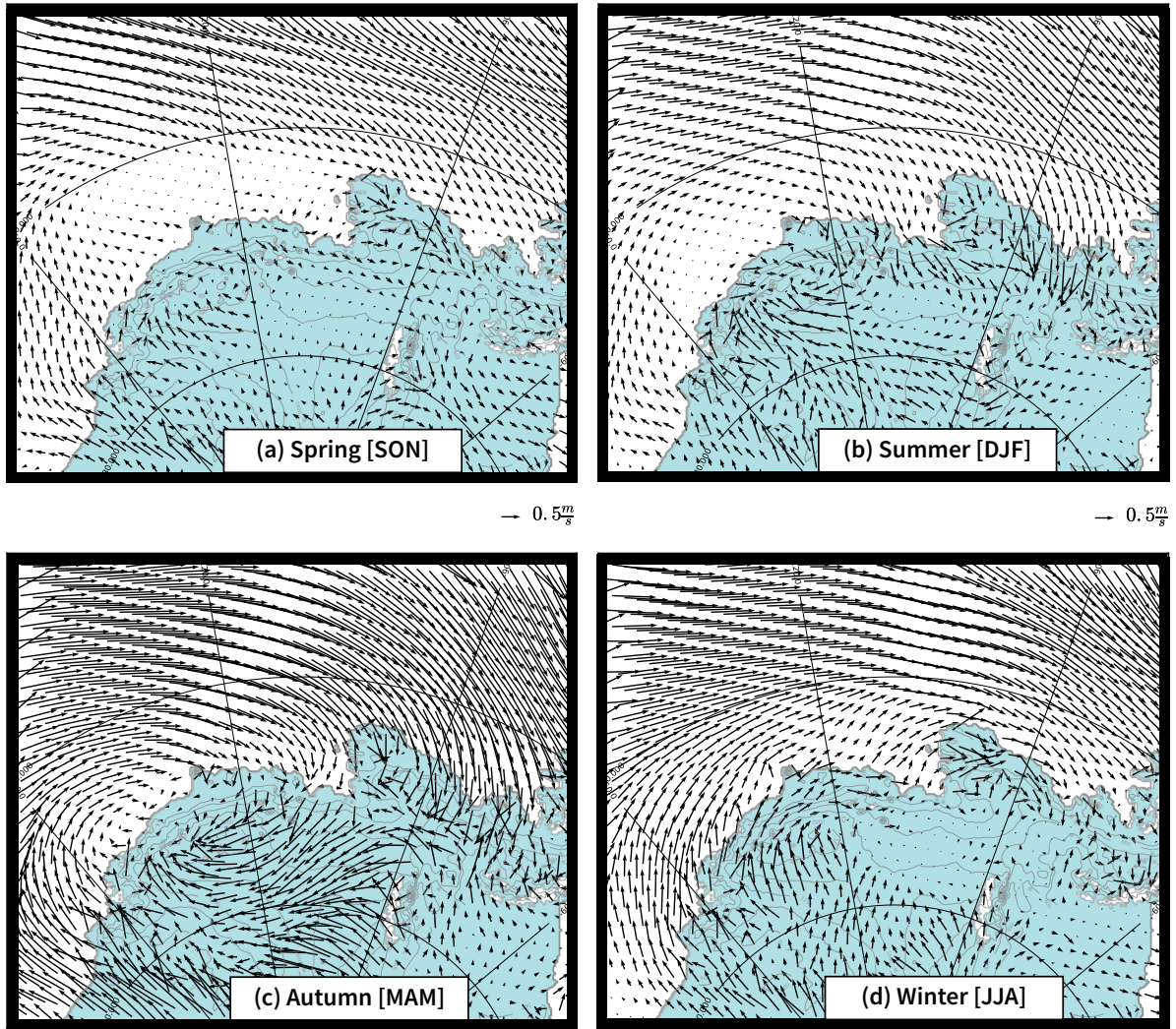


Figure 7. Changes in mean seasonal 10 m winds (future minus present). The ice sheet is in light blue and its topography is shown in gray (contours every 400 m).

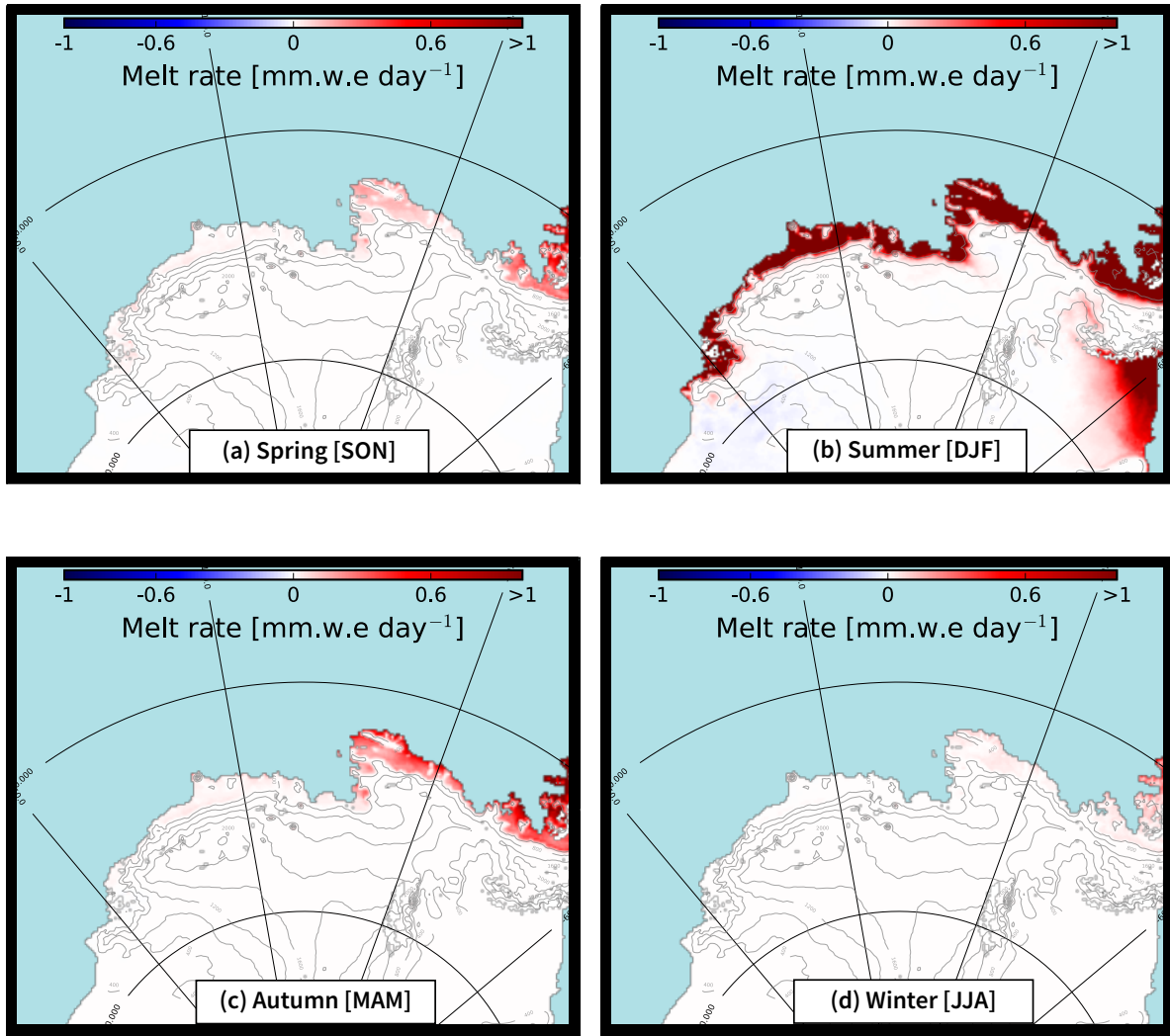


Figure 8. Changes in seasonal mean melt rates (future minus present). The ocean is in light blue, and the ice-sheet topography is shown in gray (contours every 400 m).

Table 2. Runoff, its components, and snowfall over individual ice shelves (mm.w.e.yr^{-1}), for present day (regular) and future (bold). Runoff is the sum of melting and rainfall minus refreezing. The middle row indicates the melt to snowfall ratio. The bottom rows indicate the number of rain days (threshold of $1 \text{ mm.w.e.day}^{-1}$) and the number of melt days (threshold of $3 \text{ mm.w.e.day}^{-1}$ as in Donat-Magnin et al., 2020) per year.

| Runoff component | Abbot | Cosgrove | Pine Island | Thwaites | Crosson | Dotson | Getz |
|------------------|-------------|-------------|-------------|-------------|-------------|-------------|-------------|
| Melting | 54 | 80 | 79 | 26 | 17 | 21 | 22 |
| | 577 | 588 | 455 | 244 | 183 | 292 | 333 |
| Refreezing | 60 | 83 | 85 | 29 | 20 | 24 | 25 |
| | 613 | 462 | 372 | 268 | 201 | 310 | 348 |
| Rainfall | 6 | 3 | 6 | 3 | 3 | 3 | 2 |
| | 77 | 27 | 33 | 25 | 18 | 18 | 17 |
| Runoff | 0 | 0 | 0 | 0 | 0 | 0 | 0 |
| | 40 | 153 | 116 | 0 | 0 | 0 | 1 |
| Snowfall | 790 | 290 | 407 | 809 | 1055 | 669 | 786 |
| | 943 | 372 | 521 | 989 | 1339 | 830 | 978 |
| Melt / Snowfall | 0.07 | 0.28 | 0.19 | 0.03 | 0.02 | 0.03 | 0.03 |
| | 0.61 | 1.58 | 0.87 | 0.25 | 0.13 | 0.35 | 0.34 |
| Nb rain days /yr | 1.0 | 0.6 | 1.0 | 0.5 | 0.4 | 0.3 | 0.4 |
| | 14.0 | 5.7 | 5.8 | 4.2 | 3.1 | 2.9 | 3.1 |
| Nb melt days /yr | 7.8 | 10.7 | 10.2 | 3.5 | 2.3 | 2.9 | 3.1 |
| | 65.3 | 63.2 | 46.6 | 31.0 | 25.3 | 38.0 | 42.7 |

to-snowfall ratios greater than ~ 0.85 . The existence of such a threshold explains the runoff variations across the ice shelves (middle row of Tab. 2): Abbot, Cosgrove and Pine Island have relatively high future melt rates ($\sim 0.5 \text{ m.w.e.yr}^{-1}$) but Abbot receives much higher snowfall, which explains that surface melting produces less runoff than over Cosgrove and Pine Island; the four other ice shelves experience both relatively high snowfall and weak melt rates, which explains the absence of runoff in a warmer climate. Concerning Pine Island, it should be noted that high melt rates are concentrated on its north-eastern flank

(Figs. 5,8), so related possible hydrofracturing may be limited to that part, which is not the most important in terms of ice sheet dynamics and instability (e.g. Favier et al., 2014).

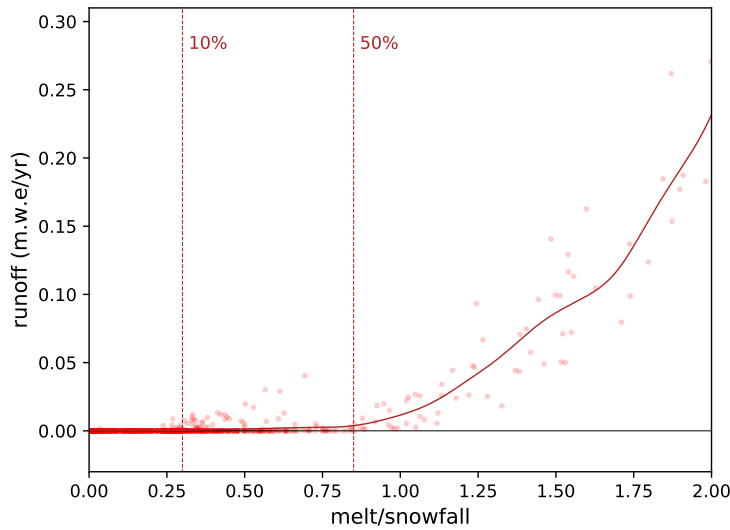


Figure 9. Runoff vs melt-to-snowfall ratio in the future simulation. Each circle represents the annual mean at a grid point within the seven glacial drainage basins. The solid curve is a Gaussian kernel density estimate with a standard deviation of 0.1 melt-to-snowfall ratio. The vertical dashed lines indicate the limit above which more than 10% and 50% of the points experience a runoff greater than 1 mm.w.e.yr^{-1} .

We now briefly analyze the causes for increased melting in a warmer climate. All along the melting season, less energy is lost by the ice-shelf surface through longwave radiation in the future (Fig. 10c), which is a consequence of higher downward longwave radiation, as expected in the presence of higher specific humidity, only partly compensated by higher upward longwave radiation emitted by a warmer snow surface in the future (Fig. 10a). In the future, more energy is also received by the snow surface through shortwave radiative fluxes over the melting season (Fig. 10d), which is explained by a melt-albedo feedback, i.e. a decreased ice-shelf albedo in the presence of more melting (Fig. 10e). These changes are partly compensated by less shortwave radiation received by the snow surface (negative anomaly of the downward component in Fig. 10a), which is explained by increased cloudiness (not shown) in the future. Changes in sensible and latent heat fluxes are less important than changes in radiative forcing, but they compensate a part of the increased longwave and shortwave radiations (Fig. 10a,b). This may be related to a thicker planetary boundary layer in the future (Fig. 10f), i.e. reduced near-surface temperature and humidity vertical gradients.

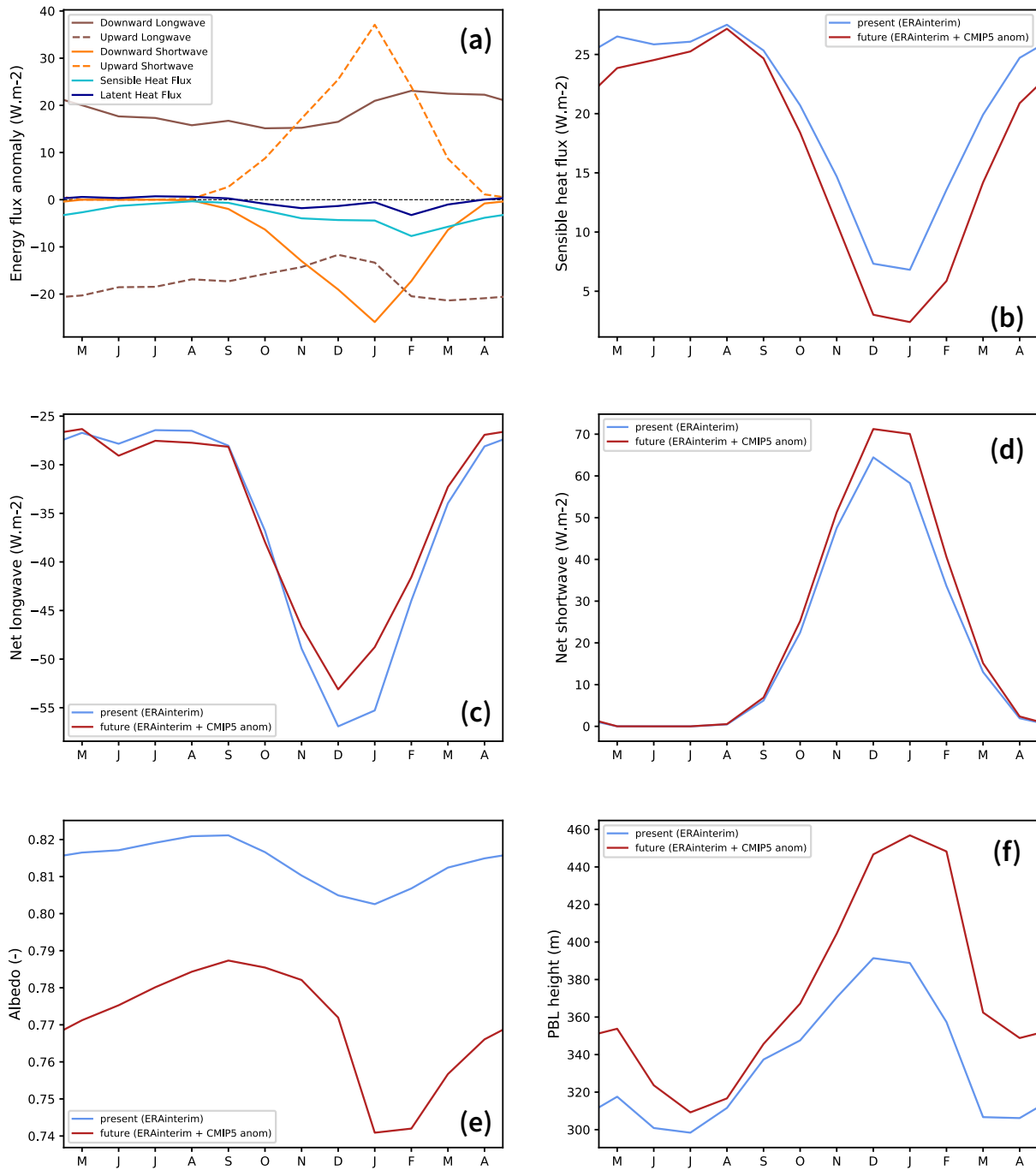


Figure 10. (a) Seasonal cycle of the anomaly (future minus present) in energy fluxes received by the ice-shelf surface (averaged over the seven major ice shelves from Getz to Abbot; positive if received by the surface). Present and future (b) sensible heat, (c) net longwave radiative, and (d) net shortwave radiative fluxes received by the ice-shelf surface. Mean present and future (e) albedo and (f) planetary-boundary-layer (PBL) height averaged over the seven major ice shelves from Getz to Abbot. The PBL height is calculated online in MAR from the vertical profile of horizontal turbulent kinetic energy.

5 Discussion

We now discuss a few limitations related to our modelling approach, then we will discuss the possibility to extend our findings to climate anomalies for other scenarios or further in time.

A critical aspect of firn modelling is the spin-up duration. Our approach has consisted of running a present and a future 5 30-year snapshot, which means that the future firn has not experienced transient changes throughout the 21st century. Instead, we have run a 12-year spin up under future conditions for every simulated year of the future experiment (the years are run in parallel). We now consider runoff in DJF 1998, which is the summer with highest melt rates in our simulation and is preceded by a decade with relatively high melt rates (Donat-Magnin et al., 2020). We consider that the spin up duration is sufficiently long if the DJF-1998 runoff reaches a steady state for spin-up durations shorter than 12 years. Whatever the spin-up duration, 10 there is no significant runoff at the surface of Getz, Dotson, Crosson and Thwaites (Fig. 11), which is expected due to the low melt-to-snowfall ratio (see previous section). For Pine Island and Cosgrove, an approximate steady state seems to be reached after 6-7 years, although runoff at Cosgrove still experiences fluctuations of $\pm 10\%$. In contrast, the runoff over Abbot is still drifting after 12 years of spin up. This is likely related to the relatively weak but non-zero runoff associated with a melt-to-snowfall ratio close to the critical threshold, which probably means that some firn columns are still slowly filling up after 15 12 years. Expanding the spin-up duration much further under constant 2080-2100 conditions would not make a lot of sense as earlier conditions were less affected by climate warming. We suggest that simulating the transient 21st century may be needed to set up the future firn properties of Abbot, and our results concerning this ice shelf have therefore to be considered carefully or discarded.

We now discuss the consequences of model and methodological biases for future runoff. Our projection method produces 20 an underestimation of both snowfall and melt rates in the future (by 16-17%, see section 3). Adding 17% to both snowfall and melting values in Tab. 2 would keep the melt-to-snowfall ratio unchanged. As such, the projection bias is not expected to change the list of ice shelves experiencing future runoff, nor the runoff intensity itself. Besides, the melt rates and snowfall produced by MAR in this configuration were shown to be biased by typically -20% and $+20\%$ respectively (Donat-Magnin et al., 2020), although observational melt-rate products are also highly uncertain (Datta et al., 2019). Increasing melt rates 25 in Tab. 2 by 20% and reducing snowfall by 20% changes the melt-to-snowfall ratios, bringing Abbot's to 0.92, well above the threshold. This again shows the high sensitivity of projected runoff at the surface of Abbot. Nonetheless, Thwaites (ratio changed to 0.37), Crosson (0.20), Dotson (0.53) and Getz (0.51) keep a low probability to experience widespread runoff even accounting for possible model biases. These estimates suggest that the absence of widespread runoff at the surface of Thwaites, Crosson, Dotson and Getz in 2100 under CMIP5-MMM-rcp8.5 conditions is a robust feature.

30 While CMIP5-MMM-rcp8.5 at the end of the 21st century is meaningful, it may be interesting to estimate the likelihood of widespread ice-shelf runoff further in the future or following alternative emission scenarios. To do so, we evaluate the

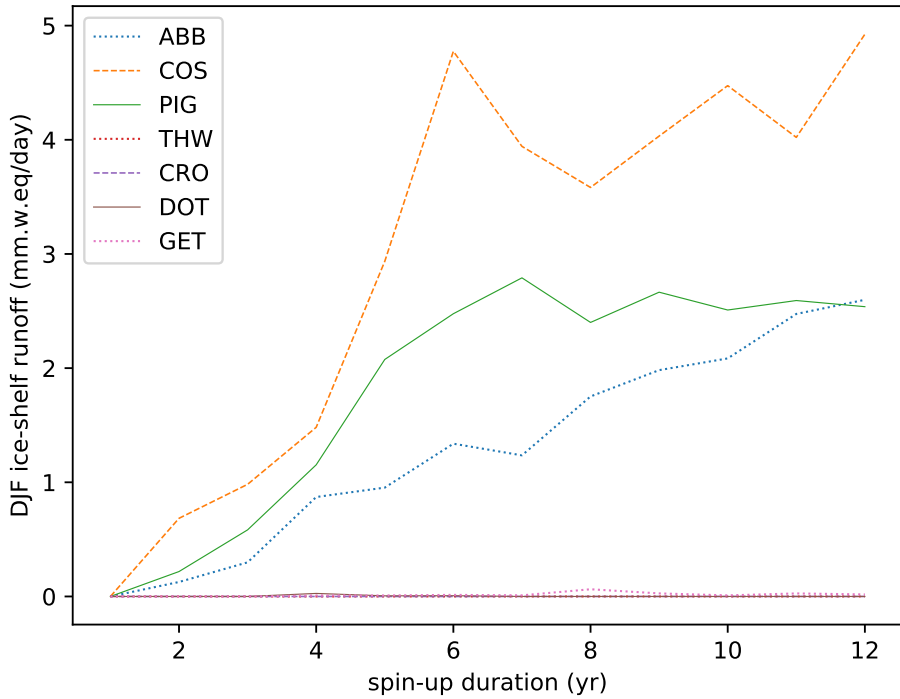


Figure 11. Ice-shelf runoff in DJF 1998 for various spin-up durations.

melt-to-snowfall ratio for a given additional warming, assuming that SMB and melt rates evolve following these equations:

$$\left\{ \begin{array}{lcl} \text{SMB}(\Delta T) & = & \text{SMB}_p e^{\frac{17.65(\Delta T - \Delta T_p)}{243.04 - 10.0}} = \text{melt}_p e^{0.0757(\Delta T - \Delta T_p)} \\ \text{melt}(\Delta T) & = & \text{melt}_p e^{0.4557(\Delta T - \Delta T_p)} \end{array} \right. \quad (1)$$

where ΔT is a given warming from present-day (1989-2009) and ΔT_p is the CMIP5-MMM-rcp8.5 warming analyzed in this study (2080-2100 minus 1989-2009). The first line is obtained by linearizing the term in the exponential of Clausius-Clapeyron around -10°C , and imposing $\text{SMB}(\Delta T = 0) = \text{SMB}_p$, which is the simulated future SMB value in a given basin. The second line is obtained considering the temperature dependency established by Trusel et al. (2015, their Fig. 1) and imposing $\text{melt}(\Delta T = 0) = \text{melt}_p$, which is the simulated future melting value in a given basin. The resulting extrapolations are shown in Fig. 12. In terms of scenarios, these extrapolations suggest that no ice shelf would experience widespread runoff over the 21st century under the rcp2.6 scenario, and only Cosgrove would experience widespread runoff before 2100 under the rcp4.5 scenario. Under the rcp8.5 scenario, the extrapolations suggest that Cosgrove would experience widespread runoff before 2050, followed by Pine Island and Abbot before 2100. The remaining ice shelves would experience widespread runoff before 2200, except Crosson that could remain relatively runoff-free until nearly 2300.

These results are difficult to compare precisely to previous studies because different metrics and scenarios were used. Based on the CMIP3 HadCM3 model under the A1B scenario (similar global warming as CMIP5-MMM-rcp8.5 in 2100), Kuipers Munneke et al. (2014) found that 50% of the present-day firn air thickness would be depleted by \sim 2130 for Cosgrove and \sim 2085 for Abbot. Assuming that this corresponds to our 0.85 melt-to-snowfall threshold, we rather find \sim 2055 for Cosgrove and 2110-2130 for Abbot. Besides, Kuipers Munneke et al. (2014) found little firn air depletion by 2200 under A1B for all the ice shelves from Thwaites to Getz, while we find that Getz and Dotson could experience significant runoff before 2200. Trusel et al. (2015) used melt-rate thresholds (based on pre-collapse observations at Larsen B) to estimate the likelihood of ice shelf collapse in future scenarios. They found that only Abbot could reach this threshold by 2100 and only under the rcp8.5 scenario, but given the large snowfall spatial variability around Antarctica and across the Amundsen region, we believe that the melt-to-snowfall ratio is a better indicator than a melt-rate threshold for runoff and potential ice-shelf collapse.

6 Conclusion

In this study, we have presented future projections of SMB and surface melting at the end of the 21st century under the rcp8.5 scenario, based on the MAR regional model at 10 km resolution. The climate change anomaly is calculated from seasonal climatologies of a CMIP5 multi-model mean, and added to the ERA-interim reanalysis which is used for present-day boundary conditions. The use of an anomaly has the advantage to start from a weakly biased present state, and is expected to reduce future biases as most CMIP5 biases were shown to be stationary. Besides, the use of a multi-model mean is expected to cancel the biases that are not common to a majority of models. An important limitation of this method is that we assume unchanged interannual variability with respect to the mean. A perfect-model test indicates that our approach captures future changes in most variables, although leading to an underestimation of SMB and melt rate changes by 17% on average.

Considering the drainage basins of the seven major ice shelves from Getz to Abbot, and only for the grounded parts of the ice sheet, we find that SMB increases from 336 Gt.yr⁻¹ in 1989-2009 to 455 Gt.yr⁻¹ in 2080-2100, which would reduce the global sea level changing rate by 0.33 mm.yr⁻¹. Even in the future climate, SMB over the grounded ice sheet remains nearly equivalent to snowfall in this region. Snowfall increases by 8.5 to 10.5% per $^{\circ}$ C of near-surface air warming (which is similar to global warming in this region). This sensitivity is slightly larger than previous estimations for the whole ice sheet (Palerme et al., 2017; Lenaerts et al., 2016; Ligtenberg et al., 2013, and references therein), and larger than predicted by Clausis-Clapeyron (increase in water-holding capacity by 7.5%. $^{\circ}$ C⁻¹ around -10 $^{\circ}$ C). This is likely explained by a decreased sea-ice cover along the ice-sheet margin, which helps near-surface air masses to reach their maximum water-holding capacity. Changes in local circulation in autumn, and associated advection of marine air, may also favor higher SMB in the future.

Then, we have analyzed future surface melting and runoff at the surface of ice shelves because they can lead to hydrofracturing and ice-shelf collapse. At the surface of the seven major ice shelves between Getz and Abbot, future melt rates are increased by an order of magnitude compared to present day, and the average number of melt days per year in the future exceeds 30 for most ice shelves. However, most melt water refreezes in the firn, even in the future run, as previously found by Kuipers Munneke et al. (2014) and Ligtenberg et al. (2013). Hence, significant amounts of runoff (produced after depletion of

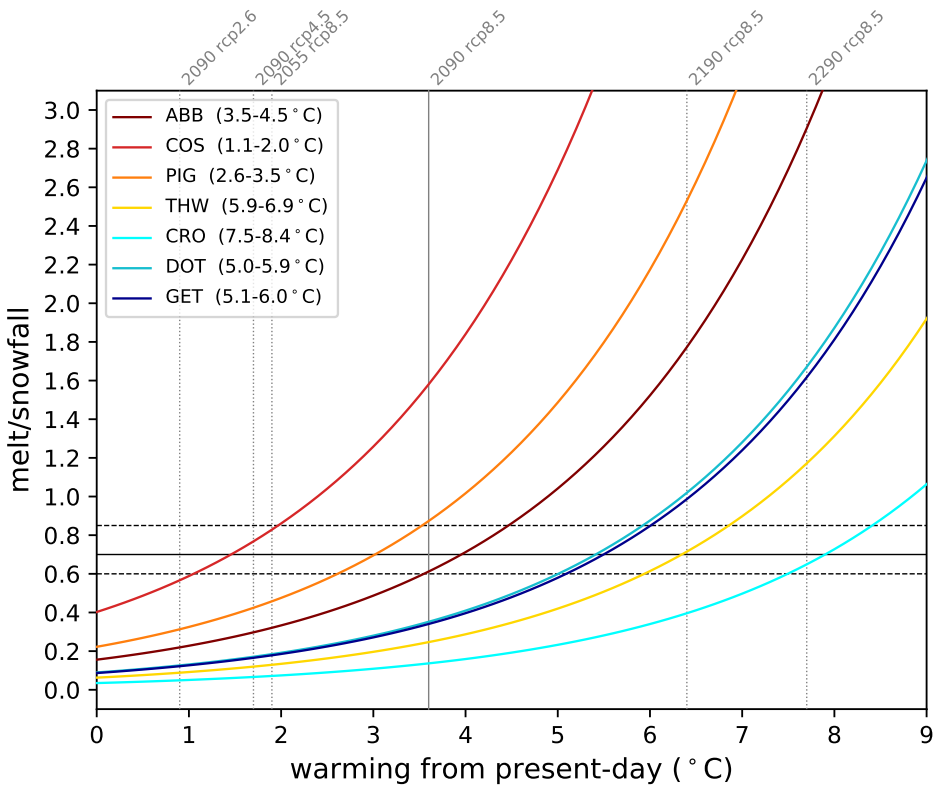


Figure 12. Extrapolated melt-to-snowfall ratio as a function of warming from present-day (see Eq. 1). The value obtained through our simulations correspond to the intersections with the gray vertical solid line. The gray vertical dashed lines represent warming at other dates (the dates indicated above the lines are the central years of 20-year averages) and under alternative scenarios (rcp2.6 and rcp4.5). This warming is derived from Collins et al. (2013, their Tab. 12.2), assuming that the regional warming remains equal to global warming (supported by our simulation results and Collins et al., 2013). The black horizontal lines indicate three indicative thresholds: the future 0.60 ratio simulated at Abbot in 2080-2100 (which is the minimum ratio for which we detect significant runoff), the 0.70 ratio estimated by Pfeffer et al. (1991), and the 0.85 ratio for which more than 50% of the grid points experience runoff (Fig. 9). The warming range for which the extrapolations cross the 0.60 and 0.85 thresholds are indicated in the figure legend.

the firn air content by melt water) are only found over Abbot, Cosgrove and Pine Island at the end of the 21st century. All the ice shelves from Thwaites to Getz are projected to remain nearly runoff-free throughout the 21st century. The melt-to-snowfall ratio explains regional contrasts in the projections, and runoff becomes significant if this ratio exceeds 0.60 to 0.85. Based on the melt and snowfall dependences to near-surface warming, we have extrapolated our projections further in time and for other scenarios. Although highly uncertain, this suggests that most ice shelves could remain runoff-free by 2100 under rcp2.6 and rcp4.5 (to the exception of Cosgrove). Under rcp8.5, the ice shelves from Thwaites to Getz may only experience widespread runoff in the second half of the 22nd century, and possibly the 23rd century in the case of Crosson. These results suggest that for Getz, Dotson, Crosson and Thwaites, ice-shelf collapse is unlikely to be triggered by hydrofracturing before the second half of the 22nd century. Nonetheless, it does not mean that these ice sheets won't collapse through other mechanisms, as observed and projected for Thwaites (e.g. Milillo et al., 2019; Yu et al., 2019).

Code availability. TO BE COMPLETED

Data availability. TO BE COMPLETED

Author contributions. M. D.-M. and N. J. initiated the study and wrote the first draft. M. D.-M. and M. C. ran the simulations. M. D.-M., C. K., Cé. A., Ch. A. and H. G. developed the model configuration. C. K. and N. J. built the surface and lateral conditions for all the future experiments. G. K. proposed the perfect-model test. All authors took part to the result discussions and to the manuscript preparation.

Competing interests. The authors declare that no competing interests are present.

Acknowledgements. The present work was funded by the French National Research Agency (ANR) through the TROIS-AS project (ANR-15-CE01-0005-01).

References

- Agosta, C., Favier, V., Krinner, G., Gallée, H., Fettweis, X., and Genthon, C.: High-resolution modelling of the Antarctic surface mass balance, application for the twentieth, twenty first and twenty second centuries, *Clim. Dyn.*, 41, 3247–3260, 2013.
- Agosta, C., Fettweis, X., and Datta, R.: Evaluation of the CMIP5 models in the aim of regional modelling of the Antarctic surface mass balance, *The Cryosphere*, 9, 2311–2321, 2015.
- 5 Agosta, C., Amory, C., Kittel, C., Orsi, A., Favier, V., Gallée, H., van den Broeke, M. R., Lenaerts, J., van Wessem, J. M., van de Berg, W. J., et al.: Estimation of the Antarctic surface mass balance using the regional climate model MAR (1979–2015) and identification of dominant processes, *The Cryosphere*, 13, 281–296, 2019.
- Bamber, J. L., Westaway, R. M., Marzeion, B., and Wouters, B.: The land ice contribution to sea level during the satellite era, *Environmental Research Letters*, 13, 063 008, 2018.
- 10 Barthel, A., Agosta, C., Little, C. M., Hatterman, T., Jourdain, N. C., Goelzer, H., Nowicki, S., Seroussi, H., Straneo, F., and Bracegirdle, T. J.: CMIP5 model selection for ISMIP6 ice sheet model forcing: Greenland and Antarctica, *The Cryosphere*, 00, 1–34, <https://doi.org/10.5194/tc-2019-191>, 2020.
- Beaumet, J., Déqué, M., Krinner, G., Agosta, C., and Alias, A.: Effect of prescribed sea surface conditions on the modern and future Antarctic 15 surface climate simulated by the ARPEGE atmosphere general circulation model, *The Cryosphere*, 13, 3023–3043, 2019a.
- Beaumet, J., Krinner, G., Déqué, M., Haarsma, R., and Li, L.: Assessing bias corrections of oceanic surface conditions for atmospheric models, *Geosci. Model Dev.*, 12, 321–342, <https://doi.org/10.5194/gmd-12-321-2019>, <https://www.geosci-model-dev.net/12/321/2019/>, 2019b.
- Bell, R. E., Chu, W., Kingslake, J., Das, I., Tedesco, M., Tinto, K. J., Zappa, C. J., Frezzotti, M., Boghosian, A., and Lee, W. S.: Antarctic 20 ice shelf potentially stabilized by export of meltwater in surface river, *Nature*, 544, 344–348, 2017.
- Bell, R. E., Banwell, A. F., Trusel, L. D., and Kingslake, J.: Antarctic surface hydrology and impacts on ice-sheet mass balance, *Nature Climate Change*, 8, 1044–1052, 2018.
- Bi, D., Dix, M., Marsland, S. J., O’Farrell, S., Rashid, H., Uotila, P., Hirst, A. C., Kowalczyk, E., Golebiewski, M., Sullivan, A., et al.: The ACCESS coupled model: description, control climate and evaluation, *Aust. Meteorol. Oceanogr. J.*, 63, 41–64, 2013.
- 25 Bracegirdle, T. J., Connolley, W. M., and Turner, J.: Antarctic climate change over the twenty first century, *J. Geophys. Res. Atmos.*, 113, 2008.
- Bracegirdle, T. J., Shuckburgh, E., Sallee, J.-B., Wang, Z., Meijers, A. J. S., Bruneau, N., Phillips, T., and Wilcox, L. J.: Assessment of surface winds over the Atlantic, Indian, and Pacific Ocean sectors of the Southern Ocean in CMIP5 models: Historical bias, forcing response, and state dependence, *J. Geophys. Res. Atmospheres*, 118, 547–562, 2013.
- 30 Bromwich, D. H., Nicolas, J. P., and Monaghan, A. J.: An assessment of precipitation changes over Antarctica and the Southern Ocean since 1989 in contemporary global reanalyses, *J. Climate*, 24, 4189–4209, 2011.
- Bull, C., Kiss, A., Sen Gupta, A., Jourdain, N. C., Argüeso, D., Di Luca, A., and Sérazin, G.: Regional versus remote atmosphere-ocean drivers of the rapid projected intensification of the East Australian Current, *J. Geophys. Res. Oceans*, submitted, 0, 0–0, 2020.
- Clapeyron, É.: Mémoire sur la puissance motrice de la chaleur, *Journal de l’École polytechnique*, 14, 153–190, 1834.
- 35 Clausius, R.: Über die bewegende Kraft der Wärme und die Gesetze, welche sich daraus für die Wärmelehre selbst ableiten lassen, *Annalen der Physik*, 155, 368–397, 1850.

- Collins, M., Knutti, R., Arblaster, J., Dufresne, J.-L., Fichefet, T., Friedlingstein, P., Gao, X., Gutowski, W. J., Johns, T., Krinner, G., Shongwe, M., Tebaldi, C., Weaver, A. J., and Wehner, M.: Long-term Climate Change: Projections, Commitments and Irreversibility. In: Climate Change 2013: The Physical Science Basis. Contribution of Working Group I to the Fifth Assessment Report of the Intergovernmental Panel on Climate Change [Stocker, T.F., D. Qin, G.-K. Plattner, M. Tignor, S.K. Allen, J. Boschung, A. Nauels, Y. Xia, V. Bex and P.M. Midgley (eds.)], Cambridge University Press, Cambridge, United Kingdom and New York, NY, USA, 2013.
- Datta, R. T., Tedesco, M., Fettweis, X., Agosta, C., Lhermitte, S., Lenaerts, J., and Wever, N.: The Effect of Foehn-Induced Surface Melt on Firn Evolution Over the Northeast Antarctic Peninsula, *Geophys. Res. Lett.*, 46, 2019.
- Davies, B. J., Golledge, N. R., Glasser, N. F., Carrivick, J. L., Ligtenberg, S. R. M., Barrand, N. E., van den Broeke, M. R., Hambrey, M. J., and Smellie, J. L.: Modelled glacier response to centennial temperature and precipitation trends on the Antarctic Peninsula, *Nature Climate Change*, 4, 993–998, 2014.
- De Ridder, K. and Gallée, H.: Land surface-induced regional climate change in southern Israel, *Journal of Applied Meteorology*, 37, 1470–1485, 1998.
- Dee, D. P., Uppala, S. M., Simmons, A. J., Berrisford, P., Poli, P., Kobayashi, S., Andrae, U., Balmaseda, M. A., Balsamo, G., Bauer, P., et al.: The ERA-Interim reanalysis: Configuration and performance of the data assimilation system, *Q. J. Roy. Meteor. Soc.*, 137, 553–597, 2011.
- Donat-Magnin, M., Jourdain, N. C., Gallée, H., Amory, C., Kittel, C., Fettweis, X., Wille, J. D., Favier, V., Drira, A., and Agosta, C.: Interannual Variability of Summer Surface Mass Balance and Surface Melting in the Amundsen Sector, West Antarctica, *The Cryosphere*, 2020.
- Dutheil, C., Bador, M., Lengaigne, M., Lefèvre, J., Jourdain, N. C., Vialard, J., Jullien, S., Peltier, A., and Menkès, C.: Impact of surface temperature biases on climate change projections of the South Pacific Convergence Zone, *Clim. Dyn.*, 53, 3197–3219, 2019.
- Favier, L., Durand, G., Cornford, S. L., Gudmundsson, G. H., Gagliardini, O., Gillet-Chaulet, F., Zwinger, T., Payne, A. J., and Le Brocq, A. M.: Retreat of Pine Island Glacier controlled by marine ice-sheet instability, *Nature Climate Change*, 4, 117–121, 2014.
- Favier, V., Krinner, G., Amory, C., Gallée, H., Beaumet, J., and Agosta, C.: Antarctica-regional climate and surface mass budget, *Current Climate Change Reports*, 3, 303–315, 2017.
- Fretwell, P., Pritchard, H. D., Vaughan, D. G., Bamber, J. L., Barrand, N. E., Bell, R., Bianchi, C., Bingham, R. G., Blankenship, D. D., Casassa, G., et al.: Bedmap2: improved ice bed, surface and thickness datasets for Antarctica, *The Cryosphere*, 7, 2013.
- Frieler, K., Clark, P. U., He, F., Buzert, C., Reese, R., Ligtenberg, S. R. M., van den Broeke, M. R., Winkelmann, R., and Levermann, A.: Consistent evidence of increasing Antarctic accumulation with warming, *Nature Climate Change*, 5, 348–352, 2015.
- Gallée, H. and Schayes, G.: Development of a three-dimensional meso- γ primitive equation model: katabatic winds simulation in the area of Terra Nova Bay, Antarctica, *Monthly Wea. Rev.*, 122, 671–685, 1994.
- Genthon, C., Krinner, G., and Castebrunet, H.: Antarctic precipitation and climate-change predictions: horizontal resolution and margin vs plateau issues, *Ann. Glaciol.*, 50, 55–60, 2009.
- Herger, N., Abramowitz, G., Knutti, R., Angélil, O., Lehmann, K., and Sanderson, B. M.: Selecting a climate model subset to optimise key ensemble properties, *Earth System Dynamics*, 9, 135–151, 2018.
- Huai, B., Wang, Y., Ding, M., Zhang, J., and Dong, X.: An assessment of recent global atmospheric reanalyses for Antarctic near surface air temperature, *Atmos. Res.*, 226, 181–191, 2019.
- Jenkins, A.: A Simple Model of the Ice Shelf–Ocean Boundary Layer and Current, *J. Phys. Oceanogr.*, 46, 1785–1803, 2016.

- Jenkins, A., Shoosmith, D., Dutrieux, P., Jacobs, S., Kim, T. W., Lee, S. H., Ha, H. K., and Stammerjohn, S.: West Antarctic Ice Sheet retreat in the Amundsen Sea driven by decadal oceanic variability, *Nature Geosc.*, 11, 733–738, 2018.
- Knutson, T. R., Sirutis, J. J., Garner, S. T., Vecchi, G. A., and Held, I. M.: Simulated reduction in Atlantic hurricane frequency under twenty-first-century warming conditions, *Nature Geoscience*, 1, 359–364, 2008.
- 5 Knutti, R., Furrer, R., Tebaldi, C., Cermak, J., and Meehl, G. A.: Challenges in combining projections from multiple climate models, *J. Climate*, 23, 2739–2758, 2010.
- Knutti, R., Sedláček, J., Sanderson, B. M., Lorenz, R., Fischer, E. M., and Eyring, V.: A climate model projection weighting scheme accounting for performance and interdependence, *Geophys. Res. Lett.*, 44, 1909–1918, 2017.
- Krinner, G. and Flanner, M. G.: Striking stationarity of large-scale climate model bias patterns under strong climate change, *Proceedings of the National Academy of Sciences*, 115, 9462–9466, 2018.
- 10 Krinner, G., Magand, O., Simmonds, I., Genton, C., and Dufresne, J.-L.: Simulated Antarctic precipitation and surface mass balance at the end of the twentieth and twenty-first centuries, *Clim. Dyn.*, 28, 215–230, 2007.
- Krinner, G., Guicherd, B., Ox, K., Genton, C., and Magand, O.: Influence of oceanic boundary conditions in simulations of Antarctic climate and surface mass balance change during the coming century, *J. Climate*, 21, 938–962, 2008.
- 15 Kuipers Munneke, P., Ligtenberg, S. R. M., Van den Broeke, M. R., and Vaughan, D. G.: Firn air depletion as a precursor of Antarctic ice-shelf collapse, *J. Glaciol.*, 60, 205–214, 2014.
- Lang, C., Fettweis, X., and Erpicum, M.: Future climate and surface mass balance of Svalbard glaciers in an RCP8.5 climate scenario: a study with the regional climate model MAR forced by MIROC5, *The Cryosphere*, 9, 945–956, 2015.
- Lenaerts, J., Ligtenberg, S. R. M., Medley, B., Van De Berg, W. J., Konrad, H., Nicolas, J. P., Van Wessem, M. J., Trusel, L. D., Mulvaney, 20 R., et al.: Climate and surface mass balance of coastal West Antarctica resolved by regional climate modelling, *Ann. Glaciol.*, 59, 29–41, 2018.
- Lenaerts, J. T. M., Van den Broeke, M. R., Van de Berg, W. J., Van Meijgaard, E., and Kuipers Munneke, P.: A new, high-resolution surface mass balance map of Antarctica (1979–2010) based on regional atmospheric climate modeling, *Geophys. Res. Lett.*, 39, 2012.
- Lenaerts, J. T. M., Vizcaino, M., Fyke, J., Van Kampenhout, L., and van den Broeke, M. R.: Present-day and future Antarctic ice sheet climate 25 and surface mass balance in the Community Earth System Model, *Clim. Dyn.*, 47, 1367–1381, 2016.
- Lewis, S. C. and Karoly, D. J.: Assessment of forced responses of the Australian Community Climate and Earth System Simulator (ACCESS) 1.3 in CMIP5 historical detection and attribution experiments, *Aust. Meteorol. Oceanogr. J.*, 64, 87–101, 2014.
- Ligtenberg, S. R. M., van de Berg, W. J., van den Broeke, M. R., Rae, J. G. L., and van Meijgaard, E.: Future surface mass balance of the Antarctic ice sheet and its influence on sea level change, simulated by a regional atmospheric climate model, *Climate dynamics*, 41, 30 867–884, 2013.
- Medley, B. and Thomas, E. R.: Increased snowfall over the Antarctic Ice Sheet mitigated twentieth-century sea-level rise, *Nature Climate Change*, 9, 34–39, 2019.
- Milillo, P., Rignot, E., Rizzoli, P., Scheuchl, B., Mouginot, J., Bueso-Bello, J., and Prats-Iraola, P.: Heterogeneous retreat and ice melt of Thwaites Glacier, West Antarctica, *Science Advances*, 5, eaau3433, 2019.
- 35 Mouginot, J., Scheuchl, B., and Rignot, E.: MEaSUREs Antarctic Boundaries for IPY 2007-2009 from Satellite Radar, Version 2, Tech. rep., Boulder, Colorado USA. NASA National Snow and Ice Data Center Distributed Active Archive Center, <https://doi.org/10.5067/AXE4121732AD>, <https://nsidc.org/data/nsidc-0709/versions/2>, 2017.

- Naughten, K. A., Meissner, K. J., Galton-Fenzi, B. K., England, M. H., Timmermann, R., and Hellmer, H. H.: Future projections of Antarctic ice shelf melting based on CMIP5 scenarios, *J. Climate*, 31, 5243–5261, 2018.
- Nicolas, J. P., Vogelmann, A. M., Scott, R. C., Wilson, A. B., Cadeddu, M. P., Bromwich, D. H., Verlinde, J., Lubin, D., Russell, L. M., Jenkinson, C., Powers, H. H., Ryczek, M., Stone, G., and Wille, J. D.: January 2016 extensive summer melt in West Antarctica favoured by strong El Niño, *Nature Communications*, 8, 15 799, 2017.
- Nowicki, S., Payne, A., Goelzer, H., Seroussi, H., Lipscomb, W., Abe-Ouchi, A., Agosta, C., Alexander, P., Asay-Davis, X., Barthel, A., Bracegirdle, T., Cullather, R., Felikson, D., Fettweis, X., Gregory, J., Hatterman, T., Jourdain, N., C., Kuipers Munneke, P., Larour, E., Little, C., Morlinghem, M., Nias, I., Shepherd, A., Simon, E., Slater, D., Smith, R., Straneo, F., Trusel, L., van den Broeke, M., and van de Wal, R.: Experimental protocol for sea level projections from ISMIP6 standalone ice sheet models, *The Cryosphere Discuss.*, 0, 0–0, 10 <https://doi.org/10.5194/tc-2019-322>, 2020.
- Palerme, C., Genthon, C., Claud, C., Kay, J. E., Wood, N. B., and L'Ecuyer, T.: Evaluation of current and projected Antarctic precipitation in CMIP5 models, *Clim. Dyn.*, 48, 225–239, 2017.
- Perlitz, J., Pawson, S., Fogt, R. L., Nielsen, J. E., and Neff, W. D.: Impact of stratospheric ozone hole recovery on Antarctic climate, *Geophys. Res. Lett.*, 35, 2008.
- Pfeffer, W. T., Meier, M. F., and Illangasekare, T. H.: Retention of Greenland runoff by refreezing: implications for projected future sea level change, *Journal of Geophysical Research: Oceans*, 96, 22 117–22 124, 1991.
- Rignot, E., Mouginot, J., Scheuchl, B., van den Broeke, M., van Wessem, M. J., and Morlighem, M.: Four decades of Antarctic Ice Sheet mass balance from 1979–2017, *Proceedings of the National Academy of Sciences*, 116, 1095–1103, 2019.
- Scambos, T., Fricker, H. A., Liu, C.-C., Bohlander, J., Fastook, J., Sargent, A., Massom, R., and Wu, A.-M.: Ice shelf disintegration by plate bending and hydro-fracture: Satellite observations and model results of the 2008 Wilkins ice shelf break-ups, *Earth Planet. Sc. Lett.*, 280, 20 51–60, 2009.
- Scott, R. C., Nicolas, J. P., Bromwich, D. H., Norris, J. R., and Lubin, D.: Meteorological drivers and large-scale climate forcing of West Antarctic surface melt, *J. Climate*, 32, 665–684, 2019.
- Seidel, D. J., Gillett, N. P., Lanzante, J. R., Shine, K. P., and Thorne, P. W.: Stratospheric temperature trends: Our evolving understanding, 25 Wiley Interdisciplinary Reviews: Climate Change, 2, 592–616, 2011.
- Shepherd, A., Ivins, E., Rignot, E., Smith, B., van den Broeke, M., Velicogna, I., Whitehouse, P., Briggs, K., Joughin, I., Krinner, G., et al.: Mass balance of the Antarctic Ice Sheet from 1992 to 2017, *Nature*, 558, 219–222, 2018.
- Swart, N. C. and Fyfe, J. C.: Observed and simulated changes in the Southern Hemisphere surface westerly wind-stress, *Geophys. Res. Lett.*, 39, 2012.
- Taylor, K. E., Stouffer, R. J., and Meehl, G. A.: An overview of CMIP5 and the experiment design, *Bul. Amer. Meteor. Soc.*, 93, 485–498, 30 2012.
- Thoma, M., Jenkins, A., Holland, D., and Jacobs, S.: Modelling circumpolar deep water intrusions on the Amundsen Sea continental shelf, Antarctica, *Geophys. Res. Lett.*, 35, 2008.
- Trusel, L. D., Frey, K. E., Das, S. B., Kuipers Munneke, P., and van den Broeke, M. R.: Satellite-based estimates of Antarctic surface 35 meltwater fluxes, *Geophys. Res. Lett.*, 40, 6148–6153, 2013.
- Trusel, L. D., Frey, K. E., Das, S. B., Karnauskas, K. B., Kuipers Munneke, P., van Meijgaard, E., and van den Broeke, M. R.: Divergent trajectories of Antarctic surface melt under two twenty-first-century climate scenarios, *Nature Geoscience*, 8, 927–932, 2015.

- Turner, J., Orr, A., Gudmundsson, G. H., Jenkins, A., Bingham, R. G., Hillenbrand, C.-D., and Bracegirdle, T. J.: Atmosphere-ocean-ice interactions in the Amundsen Sea Embayment, West Antarctica, *Rev. Geophys.*, 55, 235–276, 2017.
- van den Broeke, M.: Strong surface melting preceded collapse of Antarctic Peninsula ice shelf, *Geophys. Res. Lett.*, 32, 2005.
- van Wessem, J. M., van De Berg, W. J., Noël, B. P. Y., van Meijgaard, E., Amory, C., Birnbaum, G., Jakobs, C. L., Krüger, K., Lenaerts, J.,
5 Lhermitte, S., Ligtenberg, S. R. M., Medley, B., Reijmer, C. H., van Tricht, K., Trusel, L. D., van Ulf, L. H., Wouters, B., Wuite, J., and
van den Broeke, M. R.: Modelling the climate and surface mass balance of polar ice sheets using racmo2: Part 2: Antarctica (1979-2016),
The Cryosphere, 12, 1479–1498, 2018.
- Vaughan, D. G., Marshall, G. J., Connolley, W. M., Parkinson, C., Mulvaney, R., Hodgson, D. A., King, J. C., Pudsey, C. J., and Turner, J.:
Recent rapid regional climate warming on the Antarctic Peninsula, *Climatic change*, 60, 243–274, 2003.
- 10 Walsh, K.: Fine resolution simulations of the effect of climate change on tropical cyclones in the South Pacific, *Climate dynamics*, 45,
2619–2631, 2015.
- Yu, H., Rignot, E., Seroussi, H., Morlighem, M., and Choi, Y.: Impact of iceberg calving on the retreat of Thwaites Glacier, West Antarctica
over the next century with different calving laws and ocean thermal forcing, *Geophys. Res. Lett.*, 2019.